ChemElectroChem

Research Article
doi.org/10.1002/celc.202300393

Chemistry Europe
European Chemical Societies Publishing

www.chemelectrochem.org

New Insights into the Behaviour of Commercial Silicon Electrode Materials *via* Empirical Fitting of Galvanostatic Charge-Discharge Curves

Frederik T. Huld,*[a, b] Obinna E. Eleri,[a, b] Fengliu Lou,*[b] and Zhixin Yu*[a]

Silicon (Si) materials for use in Lithium ion batteries (LIBs) are of continued interest to battery manufacturers. With an increasing number of commercially available Si materials, evaluating their performance becomes a challenge. Here, we use an empirical fitting function presented earlier to aid in the analysis of galvanostatic charge-discharge data of commercial Si half-cells with relatively high loading. We find that the fitting procedure is capable of detecting dynamic changes in the cell, such as reversible capacity fade of the Si electrode. This fading is found to be due to the highly lithiated $Li_2Si \rightleftharpoons Li_{3.5}Si$ phase and that the behaviour is strongly dependent on the potential of this phase. EIS reveals that the Si electrode is responsible for the reversible behaviour due to progressive loss of Li^+ leading to increasing resistance. SEM/EDX and XPS characterization are also employed to determine the origin of the irreversible resistance growth on the Si electrodes.

Introduction

Commercially available silicon (Si) materials for use in lithium-ion batteries (LIBs) are a convenient way for battery manufacturers to improve their own products without the need for extremely costly and time-consuming in-house material development. Several such Si materials are already available, ranging from pure Si with capacities close to theoretical values, to heavily coated, modified, or blended materials. This poses a challenge, as comparing across materials from different suppliers is not straightforward. To fairly evaluate a given Si material therefore requires taking the intrinsic behaviour into account and analysing this to determine if it is suitable for the desired system.

A number of simple electrochemical characterization techniques are available to test Si electrodes and give information on the behaviour of the material. The most common is galvanostatic charge-discharge (GCD), whereby cells are charged and discharged in a manner similar to that experienced by full cells. This is often combined with electrochemical impedance spectroscopy (EIS) to give information about the impedances in the cell.[1,2] Non-electrochemical, *ex situ* characterization techniques such as X-ray photoelectron spectroscopy (XPS) and scanning electron microscopy (SEM) have also been employed extensively to study Si electrodes. XPS has been used to study the reaction mechanism of Si/SiO during cycling as well as studying the formation of solid electrolyte interphase (SEI) on electrodes. SEM is a common technique for determining sub-micrometre sized structural changes such as crack formation in electrodes that appear as a result of cycling.[3–5]

Despite the usefulness and pervasiveness of GCD data in the literature, surprisingly little in-depth analysis is employed to study this data. A large number of published articles only present GCD data in order to show the capacity (Q), coulombic efficiencies (CE), and differential capacity (dQ/dV) from the GCD curves. dQ/dV gives more information on the lithiation and delithiation phases present in Si but due to issues with data processing these are commonly used qualitatively, and Q and CE require just the final datapoints of the GCD curve (out of several thousand points per curve).[6–9] Gaining a better understanding of how these phases behave under different conditions will be important for designing better and more stable Si-containing LIBs.[6–10] Differential voltage (dV/dQ) is also a useful technique for studying phase transitions of materials, with the added advantage that smoothing is unnecessary.[11–13] However, the phase transitions in Si electrodes are extremely broad, making it very difficult to extract meaningful peaks from this type of analysis.

In order to extract additional information from GCD curves, empirical cumulative distribution functions (CDFs) have been developed.[6,9,14,15] These allow for the analysis of Si GCD data without the need for differentiation, thereby avoiding some of the information loss which is inevitably encountered. A CDF which has been shown to fit GCD data well even at high C-rates has been shown previously.[6] This CDF consists of a skew-Gaussian coupled with a Lorentzian to form a skew pseudo-Voigt and was shown to be able to accurately fit the delithiation phases of amorphous Si thin films as well as amorphous Si

[a] F. T. Huld, O. E. Eleri, Prof. Dr. Z. Yu
Department of Energy and Petroleum Engineering, University of Stavanger, Kjølv Egelands hus, Kristine Bonnevies vei, 4021, Stavanger, Norway
E-mail: zhixin.yu@uis.no
frederik.huld@uis.no

[b] F. T. Huld, O. E. Eleri, Dr. F. Lou
Beyonder, Stokkamyrveien 30, N-4313, Sandnes, Norway
E-mail: frederik@beyonder.no
fengliu@beyonder.no

Supporting information for this article is available on the WWW under https://doi.org/10.1002/celc.202300393

nanowires. The Lorentzian (or Cauchy) distribution is often used in combination with the Gaussian (or normal) distribution to describe spectroscopic peaks such as XPS where the use of single distributions is insufficient to explain the curve shape.[16,17] Applying this equation to commercial Si materials is a promising way to quickly gain increased understanding of both the method and the materials themselves. The empirical CDF for the capacity Q_k of Si as a function of the potential E with n delithiation phases is defined as:

$$f(E) = \sum_{k=1}^{n} Q_k[w_k G_k(E) + (1 - w_k)L_k(E)] \quad (1)$$

where $G_k(E)$ and $L_k(E)$ are the skew-Gaussian and Lorentzian components of phase k, respectively. w_k is a weighting factor ($0 \leq w \leq 1$) which determines the contribution of the skew-Gaussian or Lorentzian portions of the pseudo-Voigt CDF to the capacity of the phase. $G_k(E)$ and $L_k(E)$ are given by:

$$G_k(E) = \frac{1}{2}\left(1 + \Phi_k\left(\frac{E - c_k}{\sqrt{2}s_k}\right)\right) - 2T_k\left(\frac{E - c_k}{\sqrt{2}s_k}, \alpha_k\right) \quad (2)$$

and

$$L_k(E) = \frac{1}{\pi}\arctan\left(\frac{E - c_k}{\gamma}\right) + \frac{1}{2} \quad (3)$$

where c_k is the position (*i.e.* apparent equilibrium potential) of the phase, s_k is the width of the Skew-Gaussian, and α_k is the skewness factor describing the deviation from equilibrium.[6,18] In Eq. (3), γ_k is the width of the Lorentzian. There are advantages to using an empirical equation such as this one over a theoretical model, and there are many examples of empirical equations, such as the Stefan–Boltzmann equation for thermal radiation of a blackbody, or rate equations used in chemical rate kinetics.[19,20] Firstly, the equations can be relatively simple, allowing for fast determination of important features. Secondly, they can be applied to a broad variety of datasets generated from experiments or cells which were not designed with this particular application in mind. For example, cumulative CDFs have been used on commercial cells, as well as on Si half cell data from published works.[6,15] However, the empirical nature of these equations means that the exact behaviour of the parameters involved must be determined experimentally.

Eq. (1) describes the shapes of the lithiation/delithiation phases of amorphous Si, which can be generalized by:[21–23]

$$\text{Phase I}: \quad Li_2Si \underset{0.3\ V}{\overset{0.07\ V}{\rightleftharpoons}} Li_{3.5}Si \quad (4)$$

$$\text{Phase II}: \quad Si \underset{0.48\ V}{\overset{0.2\ V}{\rightleftharpoons}} Li_2Si \quad (5)$$

The behaviour of these two phases (n = 2) has previously been shown to vary depending on factors such as morphology and C-rate.[6] Further, the use of lithium (Li) metal as counter electrode (CE) for studying Si has been shown to have significant effect on the results.[1,24–26] Phase I (Eq. (4)) exists at low potentials *vs* Li/Li^+, forming $Li_{3.5}Si$ at 0.07 V during lithiation and Li_2Si at around 0.3 V during delithiation. Phase II (Eq. (5)) exists at higher potentials (again *vs* Li/Li^+), forming Li_2Si at 0.2 V, and delithiating to Si at around 0.48 V. We note that these values are approximations, calculated from the maxima of the dQ/dV, and vary depending on the electrochemical and physical environment of the cell (intrinsic and extrinsic resistances, material morphologies, electrode setup, current density, state of health, etc.).[6,9,15] For example, the delithiation dQ/dV of Si nanowires display sharper and less skewed peaks at 0.3 V than thin films of similar thicknesses.[6] This is also why the position of the phase c is deemed an "apparent" equilibrium potential in the literature.[6] Note that due to the presence of the skewness factor α in Eq. (2), the position of the phase c is not the same as the maximum point of the peak in a plot of dQ/dV *vs* V.

In this work we will apply Eq. (1) to the delithiation of GCD cycling data from electrodes constructed using a commercially available Si material at an electrode loading higher than what is typically observed in the literature.[6,27,28] EIS will also be performed at potentials corresponding to the maxima of the dQ/dV during both the lithiation and delithiation to give additional information on the behaviour of Si. SEM with energy-dispersive X-ray spectroscopy (EDX) and XPS will be used to validate the results of the GCD analysis.

Results and Discussion

Inspection of the GCD curves during the three formation cycles of the commercial Si revealed a number of phases consistent with graphite, indicating that the material contains a relatively large amount of carbon (C).[29] This change is shown in the supplementary information (SI) in Figure S1. However, these phases quickly disappeared as cycling progressed and only the Si phases and a capacitive component were detectable in the GCD curves after formation. This capacitive component was subtracted prior to GCD fitting by applying a linear baseline to the data. The reversible capacity of the first cycle was 520 ± 10 mAh/g and the initial Coulombic efficiency (ICE) was 74 ± 0.4 %, indicating that the material likely contains some oxides such as SiO_x. Both of these values are slightly lower than those supplied be the manufacturer (655 mAh/g and 83.7 %, respectively), but this is likely due to the somewhat higher cut-off potential used for lithiation in these experiments than those recommended by the manufacturer. This also means that the majority of the ICE loss can be ascribed to Si-related side reactions occurring above 0.05 V, with the missing capacity belonging to the graphite below 0.05 V. The results presented here should therefore not be used to judge the quality of the chosen Si material, but rather be treated as a general study into the behaviour of any given Si material.

Figure 1 shows the results of the electrochemical experiments. Figure 1a is a plot of the capacity and CE as a function of cycle number. The crosses denote the total capacity of the slow CV charging and discharging step used for the EIS experiment (shown in Figure 1b), while the points denote the much faster C/3 cycles. The reversible capacity is relatively low

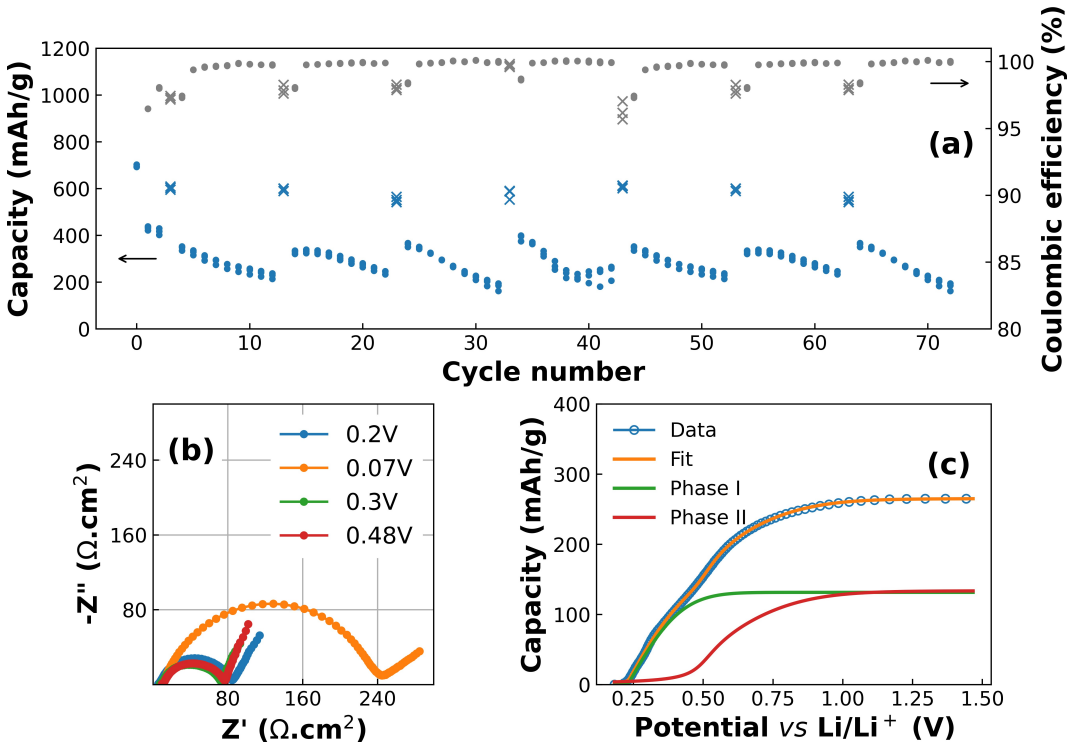

Figure 1. (**a**) Capacity (blue) and Couloumbic efficiency (grey) as a function of cycle life. The crosses denote the slow cycles used for generating EIS spectra, while the points denote the faster cycles used for GCD fitting. (**b**) EIS spectra generated at 4 potentials in the GCD curve. (**c**) An example of the fitting function applied to the GCD curves along with the shapes of the individual phases.

compared to pure Si (3579 mAh/g),[30] indicating that the material consists of a significant proportion of graphite. The cycles at C/3 show that the capacity of the electrodes fades quite quickly over the course of each group of 10 cycles, but that this capacity recovers almost completely after a slow cycle. This indicates that the cell capacity loss is not completely irreversible, at least in the short term. The CE of the slow CV cycle is quite consistently 2–2.5% lower that the much faster C/3 cycles (97.5% *vs* >99.5%) indicating incomplete delithiation of the Si electrode. The exception to this rule is the fast cycle immediately after each slow cycle, which has a CE similar to that of the preceding slow cycle. An example of the EIS spectra collected during the slow cycle (denoted by crosses in Figure 1a) is given in Figure 1b. This shows how the EIS changes depending on the potential, with the spectrum at 0.07 V in particular showing a very large impedance loop due to the Li (CE).[1,24,31] Figure 1c shows an example of one of the C/3 cycles in Figure 1a after baseline subtraction against the potential (*vs* Li/Li^+). The orange line denotes the fit of Eq. (1) to the data and the offset red and green lines correspond to phases I (Eq. (4)) and II (Eq. (5)), respectively. The raw GCD curve, together with the fit and residual can be found in Figure S2 in the SI. The residual shows an excellent fit to the data, with the difference between the fit and the data consistently below 1%.

Results of fitting Eq. (1) to the fast GCD curves is given in Figure 2. Figure 2a shows the dQ/dV curves of the first group of 10 cycles at C/3. The full spectrum is shown as grey curve, while the phases are offset for clarity. The points and diamonds

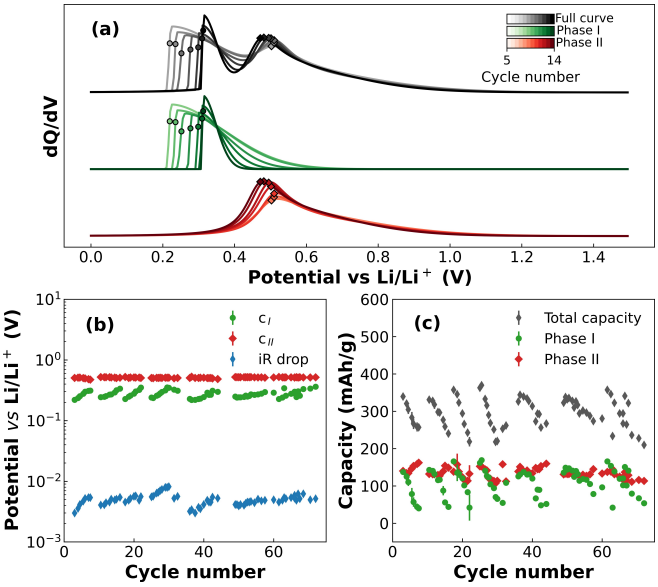

Figure 2. Results of fitting Eq. (1) to the GCD data. (**a**) Total dQ/dV of the first ten cycles at C/3 (grey lines) and the component phases (green and red for phases I and II, respectively). Darker lines correspond to later cycles. The points and diamonds denote the location of the apparent equilibrium potentials c_I and c_{II}, respectively. (**b**) Comparison between the iR drop immediately after the start of delithiation and the apparent equilibrium potentials c_I and c_{II}, as a function of the cycle number. (**c**) Total capacity of the cells along with the capacities of the individual phases, as a function of cycle number.

correspond to the apparent equilibrium potentials c_I and c_{II}, respectively. This show large changes in phase I as cycling progresses with c_I being pushed to higher potentials, causing narrowing of the phase and a decrease in the capacity (*i.e.* the area under the curve). Conversely, phase II is stable with a relatively small decrease in c_{II} and an associated increase in capacity as a function of cycling, as shown in Figure 2b and 2c, respectively. Figure 2b shows the equilibrium potentials c_I and c_{II}, along with the iR drop (calculated by taking the difference in potential between the 0th and 2nd datapoints), while Figure 2c shows the total capacity along with the capacities of the phases. From Figure 2b it can be seen that the apparent equilibrium potential of phase I, c_I, is proportional to the iR drop V_{iR}. Indeed:

$$\frac{c_I}{V_{iR}} \approx 60 \tag{6}$$

which results in a reduced χ^2 of about 0.02. However, this relationship fails at later cycles, indicating that other factors are affecting the relationship between c_I and V_{iR}. Nevertheless it is clear that V_{iR} has a large effect on the behaviour of phase I. By comparison, the apparent equilibrium potential of phase II (c_{II}) is almost constant with repeated cycling, indicating that V_{iR} is not acting upon it in the same manner. The increase in c_I is correlated with the decrease in total capacity of phase I as shown in Figure 2c. This shows that the capacity decrease of each batch of 10 cycles mostly stems from the drop in capacity of phase I, with the capacity of phase II remaining almost constant. The small increase in capacity of phase II seen at the end of each of the batches may be due to the model attempting to compensate for the large loss of capacity of phase I. The results of the fitting equation show that the total capacity of the Si material is strongly affected by the position of phase I, and that this can be correlated to the iR drop V_{iR}. The fact that this effect is somewhat reversible by applying a slow cycle means that V_{iR} is not only due to irreversible resistance growth such as SEI on the Si electrode and the overpotential of the Li CE, but also due to reversible resistance growth in the potential region of phase I. The ability of the fitting function to discern and measure these dynamic changes in the cell is therefore a valuable addition to the toolset available for studying Si electrochemistry.

Determining the origin of this reversible resistance growth is very important to interpreting the data and understanding the behaviour of Si half cells such as these. By performing EIS at the maxima of the dQ/dV, it may be possible to glean some insight into the behaviour of the cells at these potentials. The long (20 h) CV step used in the experimental setup of the EIS cycle is intended to ensure that the composition of the Si electrode is at equilibrium and that the Si in the electrode is almost completely made up of the product of the target phase (shown in bold):

$$0.2\ \text{V}: \ \text{Si} \rightarrow \mathbf{Li_2Si} \tag{7}$$

$$0.07\ \text{V}: \ \text{Li}_2\text{Si} \rightarrow \mathbf{Li_{3.5}Si} \tag{8}$$

$$0.3\ \text{V}: \ \text{Li}_{3.5}\text{Si} \rightarrow \mathbf{Li_2Si} \tag{9}$$

$$0.48\ \text{V}: \ \text{Li}_2\text{Si} \rightarrow \mathbf{Si} \tag{10}$$

This can be verified by looking at the capacity of the cycle as a function of time, as shown in Figure 3a. This shows that while most of the reactions have reached equilibrium at the end of the 20 h CV step (as evidenced by the slope tending towards 0), the reaction shown in Eq. (8) is not only far from equilibrated even after 20 h, but also varies significantly as cycling progresses. This behaviour is reflected in the EIS, which shows an increase in the impedance at the same cycle (cycle 21) as the drop in capacity, as well as subsequent decrease in impedance as the capacity recovers at later cycles. The EIS spectra generated at Eq. (8) are shown in Figure 3b, which show a large increase in impedance during the first 30 cycles, followed by a sharp decrease in subsequent cycles. This confirms that the capacity decrease seen in Figure 2 is due to the impedance of phase I during lithiation. Having shown that a reversible resistance growth contributes to the drop in capacity of Si half cells, the question of the origin of this resistance remains. This can be elucidated by analysing the distribution of relaxation times (DRT).[1,24,32] DRT analysis is a method for de-convoluting the time constants τ of an EIS spectrum. This technique relies upon the assumption that the response of an electrochemical system to a perturbation (such as an oscillating potential) decays exponentially at a particular distribution of timescales.[32] This means that an EIS spectrum can be transformed into a set of peaks corresponding to frequencies at which physical processes occur. For near-ideal processes such as corrosion on a flat surface which can be described by a resistor (R) and a capacitor (Z_C) in parallel, the peak height and the frequency $f = 1/(2\pi\tau)$ can be used to calculate R and Z_C, respectively. However in most cases the relaxation time of a process is a distribution rather than a single value, and so the width of the peak is increased. It should also be noted that DRT analysis requires the EIS spectrum to converge to the real impedance at $f = 0$. Since low-frequency diffusion effects are often present in LIBs this is rarely the case for real systems. Hence, the low-frequency region needs to be removed from consideration, either through subtraction from the data using a model equivalent circuit, or by requiring the analysis to converge to the real impedance.[1,32] Here we employ the second method and use a Gaussian Process developed earlier to perform DRT analysis on our data.[32] The results of the DRT analysis at 0.07 V are shown in Figure 3c, and these show large changes in the peak at 10^3 Hz associated with the Li CE.[1,24] Over the course of the first 21 cycles this peak grows and shifts to slightly lower frequencies, but after this point the trend reverses and the peak shrinks and shifts to higher frequencies. This may be explained by crack formation in the SEI leading to reduced Li^+ diffusion resistance.[33] This also explains the shift in frequency of the peak, as decreased inhomogeneity also increases the frequency at which Li^+ transport processes occur.[1] This, combined with a lack of a strong Si peak normally

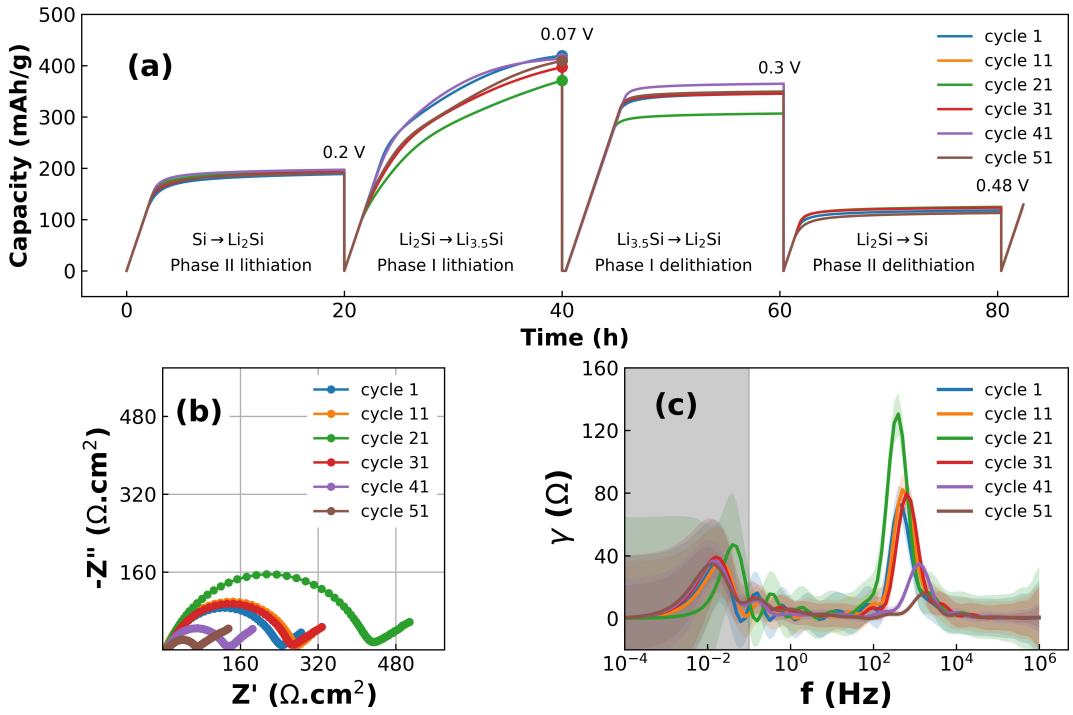

Figure 3. Results of performing EIS on Si half cells. (**a**) The capacity as a function of time for the slow cycle used for EIS. The circles at 40 h denote the point in time at which the EIS spectra displayed in (**b**) were collected. (**b**) EIS spectra taken at the end of the 0.07 V step. (**c**) DRT of the EIS spectra shown in (**b**). The shape of the curves in the greyed out area are artefacts of the analysis.

found at about 10^2 Hz means that the majority of the impedance behaviour of the half cells at a potential of 0.07 V can be ascribed to the impedances of the Li CE. However, given that the impedance decreases after the 21st cycle, the Li electrode cannot account for the reversible resistance increase seen from the GCD data which suggests that the reversible resistance stems from the Si electrode.

One possible source of this reversible resistance growth may be due to the progressive loss of Li^+ ions from the Si electrode.[6,34] The discrepancy between the capacity fade and the high CE of the fast cycles shown in Figure 1a, together with the reversible nature of the fade indicate that the cause is due to the lithiation step rather than the delithiation. Also, the fade is not due to excess SEI formation, as this would be reflected in a lowered CE. The results of the fitting shown in Figure 2c indicate that the capacity loss is due to phase I, which means that the lithiation of this phase is hindered at fast cycles. During fast lithiation the irreversible resistances of the cell (i.e. the SEI + Li CE overpotential + other resistances) result in a polarization of the cell which causes phase I (Eq. (8)) to not become fully lithiated. This therefore also causes a decrease in capacity of phase I during delithiation (Eq. (9)), which is measured by Eq. (1). Since the resistance of the Si electrode is inversely proportional to the Li concentration in Si, the subsequent cycle experiences an increased resistance, and therefore decreased lithiation. This leads to a negative feedback loop wherein the amount of Li^+ inserted into phase I continuously decreases. Applying a slow cycle such as the one employed for studying the EIS increases the Li^+ content in the electrode and decreases V_{iR}), which "resets" the Si electrode and therefore allows the capacity to recover.

This indicates that reducing the cell resistances may substantially improve the performance of Si materials independently of the material itself, and that the capacity fade is a result of both reversible and irreversible resistances. As seen from the EIS results at low potentials *vs* Li/Li^+, the Li CE accounts for a large portion of this resistance. Thus, high-capacity materials, and especially those with high electrode loading will be artificially hindered by the Li CE due to the large current densities required to cycle at appreciable rates.[25] Further, constructing cells with higher areas will also likely increase the performance of Si cells purely through the decrease in area resistance.

Unfortunately, the dynamic nature of this resistance growth means that it is very difficult to measure it directly. The steady-state nature of experiments such as EIS and *ex-situ* experiments such as SEM/EDX and XPS means that they are only able to measure the irreversible resistances. Nevertheless, they are a valuable tool to gain a deeper understanding of the behaviour of the system. To show that the irreversible SEI resistance is growing on the Si electrode with time, SEM/EDX and XPS analysis was carried out on fresh, uncycled electrodes as well as electrodes disassembled at the end of cycling. The results of the SEM analysis can be found in Figure 4. The uncycled electrode (Figure 4a) shows how the Si electrode is made up of large micron-sized graphite/carbon particles, mixed with agglomerations of small spherical Si particles. The long fibres covering the surface are the CNTs added to the electrode to improve the conductivity. The cycled electrode in Figure 4b is coated in a

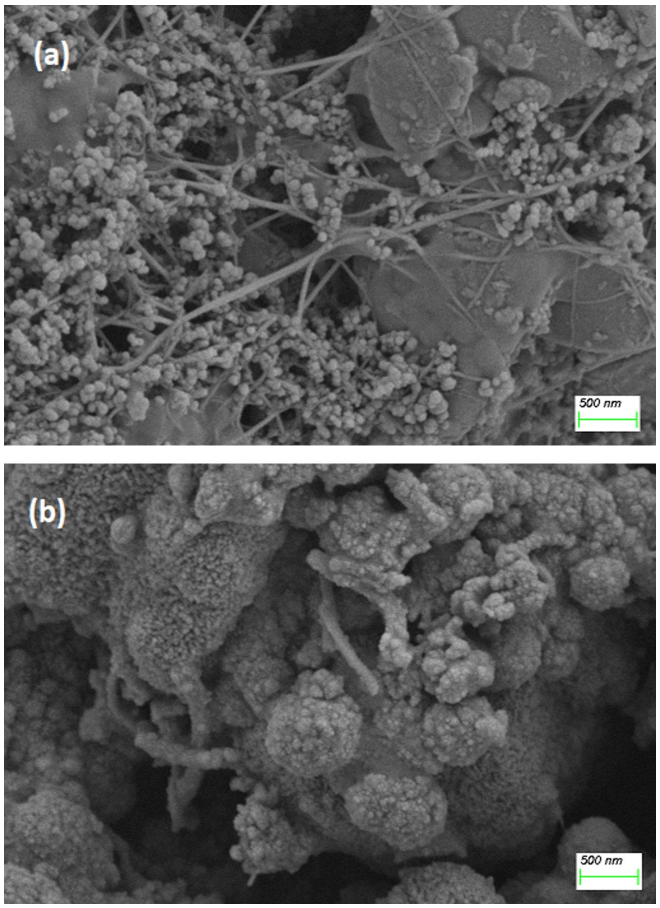

Figure 4. SEM images of Si electrodes (**a**) before and (**b**) after cycling.

layer of SEI, indicating that the anode is at least partially responsible for the irreversible resistance increase seen in the GCD data. Spot EDX analysis (Figure 5a) from SEM on cycled and uncycled electrodes shows a reduction of the C peak and an increase in the oxygen (O), fluorine (F) and phosphorus (P) peaks. This implies that the surface of the electrode is covered by inorganic O, F and P-rich species. These may consist of materials such as LiF, phosphates and lithium alkyl carbonates. This is consistent with the results of the XPS C1s spectra shown in Figure 5b and 5c for the uncycled and cycled electrodes, respectively. Figure 5b shows a large C=C graphite peak at 284.8 eV, as well as oxygen species such as carboxylic acids and ketones present on the surface of the graphite and other carbonaceous materials that make up the anode. The lack of a detectable C=C peak in the cycled electrode, shown in Figure 5c, indicates that the graphite is obscured by the presence of a passivating SEI layer. This presence of CH_x and O–C=O groups correspond to the characteristic signature of lithium alkyl carbonates, primary components of SEI.[35–37]

The increased polarization observed in both the GCD fitting and the EIS experiments can therefore be explained in part by the excessive SEI growth often seen on Si electrodes.

The relationship between the irreversible and reversible resistances are shown schematically in Figure 6. This shows how the irreversible resistances contribute to the polarization of the cell, which leads to reduced lithiation of phase I. The reduced Li^+ concentration in phase I increases the resistance of the electrode, which leads to further decreases in lithiation.

Conclusions

Commercial Si electrodes with high loading of 3.27 mAh/g were constructed in half-cell format and tested using GCD and EIS. A fitting function was applied to the delithiation steps, revealing that phase I, describing the reaction $Li_2Si \rightleftharpoons Li_{3.5}Si$ is responsible for the fast but reversible capacity fade experienced by these cells. Further analysis of the data showed a relatively linear relationship between the position of phase I and the iR drop experienced by the cell at the start of delithiation, leading to the conclusion that the capacity fade is due to polarization of the cell. EIS and DRT performed near the positions of the phases showed that the reversible resistance growth came from the Si electrode. This was explained by the concept of a "negative feedback loop" whereby the large irreversible polarizations from the Si and Li electrodes decrease the Li^+ concentration in phase I of the Si electrode. This leads to an increase in resistance of the Si electrode, which contributes to the polarization on the subsequent cycle. The irreversible resistance growth on the Si electrode was measured by performing SEM/EDX and XPS on uncycled and cycled electrodes. This work showcases the fitting function as a valuable technique for studying dynamic changes in commercial Si materials during cycling.

Experimental

Electrode slurries were prepared by high-speed stirring in a manner described previously, using SL650-SOC (Iopsilion) as the active material.[24] Electrode sheets were made by coating onto 10 μm thick copper foil using a doctor blade with a blade height of 130 μm and dried at room temperature. This yielded electrodes with a material loading of 3.27 mg/cm^2 and a thickness of 48 μm. The Si material loading was 80%; the binders consisted of 5% carboxymethylcellulose (CMC, Walcocel 10000) and 3% styrene butadiene rubber (SBR, BM-451B, Zeon) along with 2% KOH/citric acid buffer to aid the adhesion; 0.5% carbon nanotubes (CNT, Lanxi Zhide) and 9.5% carbon black (CB, Group 14) were added as conductive additives.

Coin half-cells were constructed in CR2032 format (MTI) in an Argon-filled glovebox in a manner described previously.[3] The electrolyte used was commercially available TC-E8593 (TINCI).

After assembly the coin cells were immediately discharged to 1.5 V, followed by a 12 h rest. Three formation cycles were performed in the range 0.05–1.5 V. These consisted of 1 cycle at C/20 (83 μA/cm^2) followed by 2 cycles at C/10 (0.166 mA/cm^2). The formation was followed by the slow cycle for EIS, which was performed by using a C/10, 20 h constant-current constant-voltage (CCCV) step to the desired "stop" potential. The stop potentials for lithiation were 0.2 V and 0.07 V, while for delithiation they were set to 0.3 V and 0.48 V. EIS was performed at the end of each of these stop potentials. After the slow cycle, a batch of 10 "fast" cycles at C/3 (0.55 mA/cm^2) were performed. This procedure of one slow EIS cycle and 10 fast cycles was repeated until the cells failed.

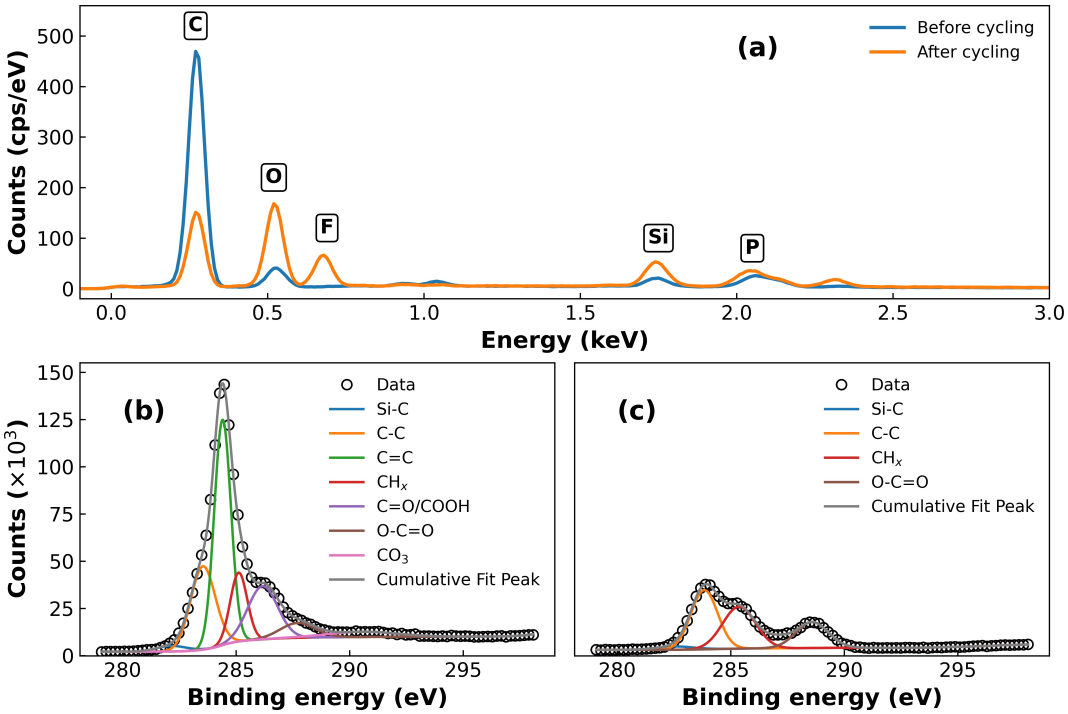

Figure 5. (**a**) Spot EDX of Si anodes before and after cycling. (**b**) XPS C1s spectrum of the Si anode before cycling. (**c**) XPS C1s spectrum of the Si anode after cycling.

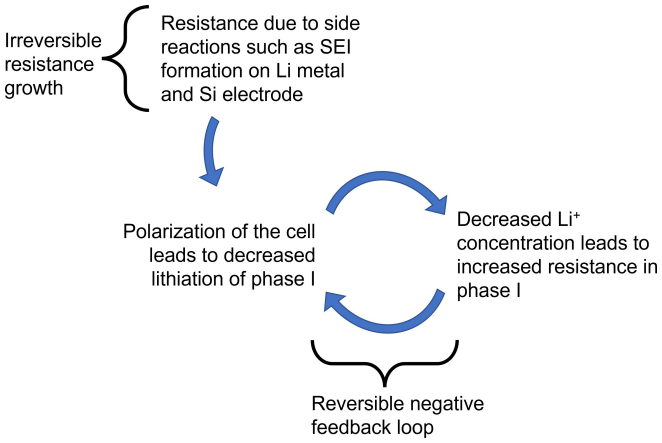

Figure 6. Schematic showing the process of irreversible and reversible resistance growth, and its relationship to the fast capacity fade seen in Si half cells.

EIS was performed on coin half cells using a potentiostat (Autolab, Metrohm). The oscillation amplitude was set to 5 mV in the frequency range of 10^5 to 10^{-2} Hz. Analysis of the spectra was performed using the impedance package in Python,[38] and distribution of relaxation times (DRT) analysis was performed in Python using the methods described by Liu and Ciucci (2020).[32]

GCD fitting was performed on the delithiation step of the fast cycles using the lmfit package in Python, as described previously.[6,39] Since the lithiation of Si occurs very close to the cut-off potential, it is not possible to accurately fit the lithiation step of the GCD curves. Therefore, only the delithiation step is fit.

Characterization *via* SEM/EDX (ZEISS/Oxford Instruments) and XPS (Thermo Fisher) was performed on both cycled and uncycled electrodes. Cycled electrodes were prepared by disassembly of cycled cells in an Argon-filled glovebox and rinsed three times in DMC before drying to remove excess electrolyte salt.

Conflict of Interests

F.T. Huld and F. Lou declare that they are employees and stockholders of Beyonder AS, a Norwegian battery company. The remaining authors do not declare a conflict of interest.

Data Availability Statement

The data that support the findings of this study are available from the corresponding author upon reasonable request.

Keywords: capacity fade · electrochemical impedance spectroscopy · incremental capacity analysis · lithium ion batteries · silicon anodes

[1] K. Pan, F. Zou, M. Canova, Y. Zhu, J.-H. Kim, *J. Power Sources* **2020**, *479*, 229083.
[2] F. Paloukis, C. Elmasides, F. Farmakis, P. Selinis, S. G. Neophytides, N. Georgoulas, *J. Power Sources* **2016**, *331*, 285.
[3] F. T. Huld, S. Y. Lai, W. M. Tucho, R. Batmaz, I. T. Jensen, S. Lu, O. E. Eleri, A. Y. Koposov, Z. Yu, F. Lou, *ChemistrySelect* **2022**, *7*, e202202857.
[4] H. Wu, L. Zheng, J. Zhan, N. Du, W. Liu, J. Ma, L. Su, L. Wang, *J. Power Sources* **2020**, *449*, 227513.
[5] S. Y. Lai, J. P. Mæhlen, T. J. Preston, M. O. Skare, M. U. Nagell, A. Ulvestad, D. Lemordant, A. Y. Koposov, *Nanoscale Adv.* **2020**, *2*, 5335.
[6] F. T. Huld, J. P. Mæhlen, C. Keller, S. Y. Lai, O. E. Eleri, A. Y. Koposov, Z. Yu, F. Lou, *Batteries* **2023**, *9*, 251.

[7] Y. Li, M. Abdel-Monem, R. Gopalakrishnan, M. Berecibar, E. Nanini-Maury, N. Omar, P. van den Bossche, J. Van Mierlo, *J. Power Sources* **2018**, *373*, 40.
[8] X. Li, Z. Wang, J. Yan, *J. Power Sources* **2019**, *421*, 56.
[9] J. He, X. Bian, L. Liu, Z. Wei, F. Yan, *J. Energy Storage* **2020**, *29*, 101400.
[10] A. J. Smith, J. R. Dahn, *J. Electrochem. Soc.* **2012**, *159*, A290.
[11] I. Bloom, A. N. Jansen, D. P. Abraham, J. Knuth, S. A. Jones, V. S. Battaglia, G. L. Henriksen, *J. Power Sources* **2005**, *139*, 295.
[12] I. Bloom, J. P. Christophersen, D. P. Abraham, K. L. Gering, *J. Power Sources* **2006**, *157*, 537.
[13] I. Bloom, L. K. Walker, J. K. Basco, D. P. Abraham, J. P. Christophersen, C. D. Ho, *J. Power Sources* **2010**, *195*, 877.
[14] X. Li, J. Jiang, L. Y. Wang, D. Chen, Y. Zhang, C. Zhang, *Appl. Energy* **2016**, *177*, 537.
[15] X. Bian, L. Liu, J. Yan, *Energy* **2019**, *177*, 57.
[16] G. K. Wertheim, M. A. Butler, K. W. West, D. N. E. Buchanan, *Rev. Sci. Instrum.* **1974**, *45*, 1369.
[17] J. Olivero, R. Longbothum, *Journal of Quantitative Spectroscopy and Radiative Transfer* **1977**, *17*, 233.
[18] M. S. Palagonia, C. Erinmwingbovo, D. Brogioli, F. La Mantia, *J. Electroanal. Chem.* **2019**, *847*, 113170.
[19] M. J. Stefan, *Über die Beziehung zwischen der Warmestrahlung und der Temperatur*, vol. 1 **1879** pages 391–428.
[20] P. W. Atkins, J. De Paula, *Atkins' Physical Chemistry*, W. H. Freeman, New York, 8th ed edition **2006**.
[21] K. Ogata, E. Salager, C. Kerr, A. Fraser, C. Ducati, A. Morris, S. Hofmann, C. Grey, *Nat. Commun.* **2014**, *5*, 3217.
[22] B. Key, M. Morcrette, J.-M. Tarascon, C. P. Grey, *J. Am. Chem. Soc.* **2011**, *133*, 503.
[23] J. Li, J. R. Dahn, *J. Electrochem. Soc.* **2007**, *154*, A156.
[24] F. Huld, Z. Yu, F. Lou, *Energy Advances* **2023**, page 10.1039.D3YA00181D.
[25] F. La Mantia, C. Wessells, H. Deshazer, Y. Cui, *Electrochem. Commun.* **2013**, *31*, 141.
[26] M. Ender, J. Illig, E. Ivers-Tiffée, *J. Electrochem. Soc.* **2017**, *164*.
[27] Z. Chen, C. Wang, J. Lopez, Z. Lu, Y. Cui, Z. Bao, *Adv. Energy Mater.* **2015**, *5*, 1401826.
[28] Y. Wang, H. Xu, X. Chen, H. Jin, J. Wang, *Energy Storage Mater.* **2021**, *38*, 121.
[29] F. Dinkelacker, P. Marzak, J. Yun, Y. Liang, A. S. Bandarenka, *ACS Appl. Mater. Interfaces* **2018**, *10*, 14063.
[30] H. Tian, F. Xin, X. Wang, W. He, W. Han, *J. Mater.* **2015**, *1*, 153.
[31] J. Seok, C. N. Gannett, S.-H. Yu, H. D. Abruña, *Anal. Chem.* **2021**, *93*, 15459.
[32] J. Liu, F. Ciucci, *Electrochim. Acta* **2020**, *331*, 135316.
[33] A. Ramasubramanian, V. Yurkiv, T. Foroozan, M. Ragone, R. Shahbazian-Yassar, F. Mashayek, *ACS Appl. Energ. Mater.* **2020**, *3*, 10560.
[34] E. Pollak, G. Salitra, V. Baranchugov, D. Aurbach, *J. Phys. Chem. C* **2007**, *111*, 11437.
[35] P. Verma, P. Maire, P. Novák, *Electrochim. Acta* **2010**, *55*, 6332.
[36] M. Smith, L. Scudiero, J. Espinal, J.-S. McEwen, M. Garcia-Perez, *Carbon* **2016**, *110*, 155.
[37] X. Chen, X. Wang, D. Fang, *Fullerenes Nanotubes Carbon Nanostruct.* **2020**, *28*, 1048.
[38] M. Murbach, B. Gerwe, N. Dawson-Elli, L.-K. Tsui, *Journal of Open Source Software* **2020**, *5*, 2349.
[39] M. Newville, R. Otten, A. Nelson, T. Stensitzki, A. Ingargiola, D. Allan, A. Fox, F. Carter, Michał, R. Osborn, D. Pustakhod, Ineuhaus, S. Weigand, A. Aristov, Glenn, C. Deil, mgunyho, Mark, A. L. R. Hansen, G. Pasquevich, L. Foks, N. Zobrist, O. Frost, Stuermer, azelcer, A. Polloreno, A. Persaud, J. H. Nielsen, M. Pompili, S. Caldwell, Lmfit/Lmfit-Py: 1.2.0, Zenodo **2023**.

Manuscript received: August 7, 2023
Revised manuscript received: September 18, 2023
Version of record online: October 12, 2023